(Received 3 November 2023, Accepted 22 December 2023, Scheduled 5 January 2024)

A Compact Dual-Band Dual-Polarized Antenna Based on Modified Minkowski Fractal

Mahmood T. Yassen[1], Ali J. Salim[2, *], Mohammed R. Hussan[2], and Jawad K. Ali[2]

[1] *Microwave Research Group, Department of Electrical Engineering, University of Technology, Iraq*
[2] *Applied Electromagnetic Group, Department of Communication Engineering, University of Technology, Iraq*

ABSTRACT: The polarization of the received signals can be effectively matched regardless of the orientation of the receiving antenna using circularly polarized antennas. A compact printed monopole antenna with a circular ring patch is presented in this paper. The proposed antenna will be able to provide two polarization states: linear and circular. The employment of a modified Minkowski fractal with 1st iteration construction on an open circular ring supports a circularly polarized band having a center frequency of 1.812 GHz and fractional bandwidth (FBW) of 20.033%. The upper band is achieved with a linearly polarized wave having a center frequency of 3.386 GHz and a fractional bandwidth of 11.399%. The proposed antenna is fed by an ungrounded co-planar waveguide (UCPW), enhanced with an impedance transformer to match at 50 Ohms with the characteristic impedance. The ground planes around the feed line are defected by ground structures to improve the antenna gain. The fabrication and measurement of the proposed antenna prototype are presented to validate the theoretical results. Measured results support the theoretical findings well.

1. INTRODUCTION

Emerging wireless devices are being developed at this age. This development must be followed by antennas with special requirements. Besides the circular polarization property for such antennas, compact size represents a crucial issue in designing modern wireless communication systems. Fractal geometry structures meet the compact size and circular polarization radiation pattern for antennas at the same time. Many research works discussed using different types of fractal geometry in designing antennas for various communication applications have been reported in the literature [1–20].

In this context, constructing fractals in circularly polarized antennas may be employed as poly structures consisting of two fractal types to achieve the circular polarization property. The Minkowski fractal curve is used for this purpose besides the Koch curve [1], half-circled fractal curve [2], ring-loaded fractal [3], and even Minkowski fractal structure [4]. The Giuseppe-Peano fractal's circular polarization (CP) antenna was applied on a square fractal as a poly fractal to generate triple resonating bands [5]. The series connection of Z-type fractal and Hilbert fractal in a zig-zag formation made the designed antenna resonate with triple bands having circular polarization and broad radiation characteristics [6]. In [7], the combination of Koch and Minkowski pre-fractal with a Y-type strip is accomplished to increase the electrical current length, which could be controlled by changing the indentation depth and angle at the boundary of the patch to decrease the resonance frequency in CP printed antenna for L-band application.

However, other types of fractals may be applied as individual forms in the design of circularly polarized antennas. For this context, the Minkowski fractal curve and the emerging technique of defected ground structure (DGS) in [8] are employed for miniaturizing an antenna by 44.7% with good circular polarization compared to the conventional circularly polarized antenna. In [9], a Minkowski fractal structure for the GPS antenna is presented to meet the requirements of satellite-receiver bandwidth, which is about 30 MHz. The circular polarization in this antenna is obtained by a corner truncated off its square patch. A compact antenna in [10] is designed by adding flared-U-type asymmetrical fractals to generate two orthogonal modes for circular polarization emission. A fractal flared-U-type structure replaces the square patch's edge for this antenna, and then the indentation parameters of the fractal boundary curves are optimized. In [11], a slot array as a circularly polarized antenna is adopted. The design process of this antenna is based on a fractal geometry known as Gasper-Peano, which represents the feedline of this antenna and an array of slots at the ground plane to form the radiating element of the structure with the assistance of mean-square-error function represented by genetic algorithm to satisfy an accepted circular polarization and high radiation efficiency.

On the other hand, embedded slots can be constructed as fractal structures to perform circular polarization characteristics [12–15]. In [12], a rhombus slot is proposed to design an antenna with miniaturized size and fed by an L-shaped feedline to give a wide 3-dB axial ratio for a single resonating band. In [13], the fractal represents simple embedded slots at cross-positions etched on the radiation element of the antenna and excited indirectly from a microstrip feedline using coupling through a small distance for RFID application designed to introduce a miniature CP antenna. The Spidron slot fractal in [14] supports circular polarization with wide axial ratio bandwidth for the designed antenna, which is supplied by a tapered

* Corresponding author: Ali Jabbar Salim (alijsalim@gmail.com).

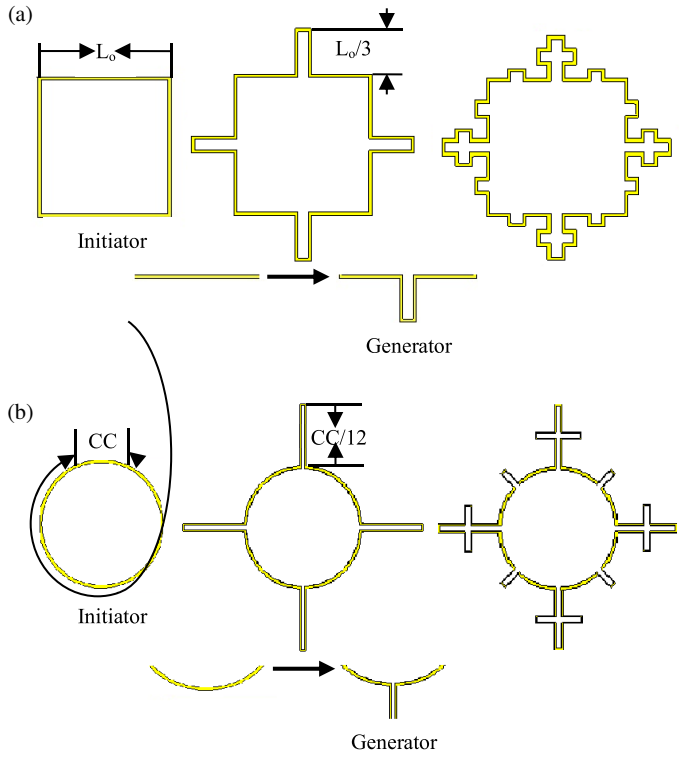

FIGURE 1. Employing modified Minkowski fractal curve up to 2nd iteration on (a) square ring and (b) circular ring.

Parameter	Parameter Description	Value in mm
L_{sub}	Substrate length	50
W_{sub}	Substrate width	50
h_{sub}	Substrate height	1.6
R_{in}	Inner circle radius	2.5
R_{ou}	Outer circle radius	5
L_f	Fractal length	2.67
W_f	Fractal width	2.5
L_s	Fractal slot length	4.35
W_s	Fractal slot width	0.65
W_{gs}	Gap slot width	1.25
L_t	Impedance transformer length	7.75
W_{rc}	Resonant cavity width	0.05
L_{fl}	Feed line length	17.25
W_{fl}	Feed line width	6.1
W_{gfl}	Feed line gap width	0.75
L_g	Ground plane length	17.5
W_g	Ground plane width	21.2
R_g	Radius of truncated circle	15
D_x	Horizontal distance offset of the DGS	4.06
D_y	Vertical distance offset of the DGS	1

TABLE 1. Description and values of antenna parameters.

microstrip feedline. Another technique in the embedded slot fractal is to develop a CP antenna known as a fractal-defected ground structure (FDGS). In this technique, a specific fractal type is etched on the ground plane, such as a tree of the Y-shape in [15], and by adjusting the dimensions of this fractal, circular polarization is achieved.

A dual-band dual-polarized antenna for GSM and WiMAX applications is designed and fabricated in this communication. The proposed antenna generates the lower resonating band with left-handed circular polarization (LHCP) radiation pattern due to the modified Minkowski fractal geometry on the open-ended circular ring patch. The upper resonating frequency band has a linear polarization radiation pattern. The proposed antenna is excited by an ungrounded co-planar waveguide (CPW). The emerging defected ground structure (DGS) technique is used symmetrically on both sides of the ground plane around the feed line.

2. MODIFIED MINKOWSKI FRACTAL AND THE ANTENNA GEOMETRY

The miniaturization of micro-wave circuit components and antenna design adopts a basic idea that increases the exciting electrical current length along a specified physical area. There are other challenges that the design may require, such as multi-band response, broadband resonance, high gain, and polarization property; therefore, the fractal geometry is considered an attractive solution to satisfy these issues.

Two main points must be considered in fractal geometry: the type of fractal that should be proposed to a specific design and the fractal dimension. Microwave passive circuit designers attempt modified fractals instead of classical fractals because the modified versions have a high fractal dimension, generating many space-filling curves, and constructing structures with more size reduction [18].

For the reasons mentioned above and the requirement of circular polarization property, a modified Minkowski fractal is applied in the proposed antenna design. Figure 1 illustrates the generation process of the modified Minkowski fractal. In Figure 1(a), the loading of fractal curves to a square ring is proceeded by replacing each side length in the ring (initiator) with a (generator) having width differs from the typical ratio (1/3 of the original length) which is commonly used in the construction of the majority of fractal curves, while Figure 1(b) shows the sequence of design steps of the modified Minkowski fractal up to the 2nd iteration on a circular ring, and in this case, the length of (generator) would be equal to or less than about 1/12 of the circumference for the circular ring.

The structure of the designed antenna is presented in Figure 2. The proposed antenna consists of an open circular ring, acts as a radiator, includes a modified Minkowski fractal curve of 1st iteration, and is supported by an impedance transformer. The feeding system of this antenna is created as a 50-ohm ungrounded co-planar waveguide (UCPW). The defected ground structure (DGS) technique etched the ground plane to form a slot on each ground plane around the feedline with a size reduction of 0.7 mm from the original dimension. The proposed an-

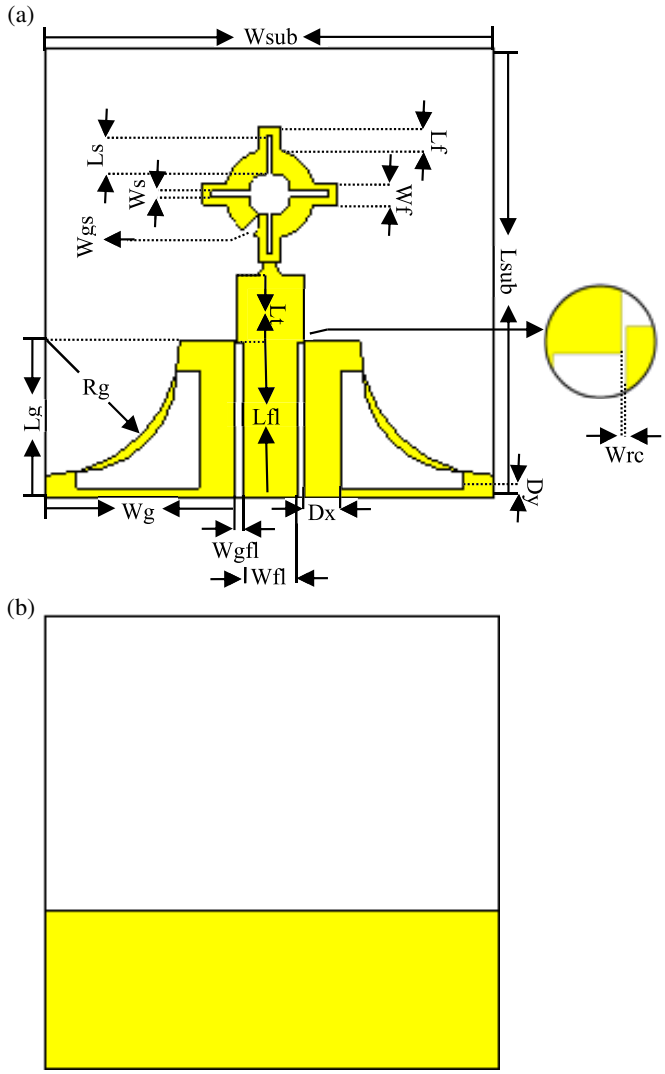

FIGURE 2. The structure of the proposed antenna: (a) Front view, (b) back view.

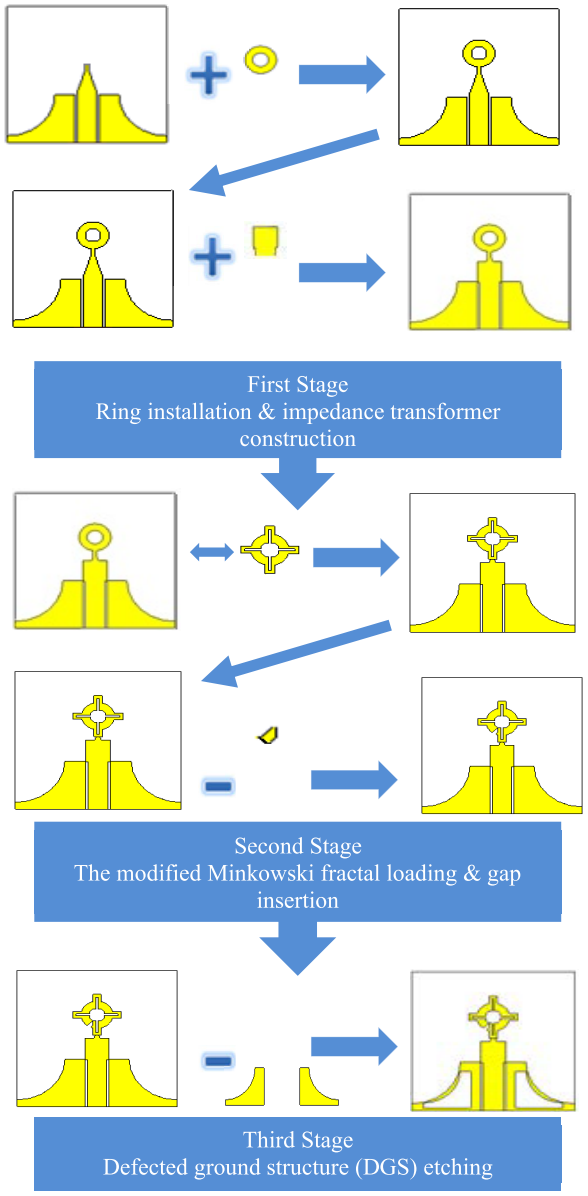

FIGURE 3. Antenna design procedure.

tenna is supposed to be printed on a compact FR-4 glass epoxy substrate with a relative permittivity of 4.4 and dimensions of $50 \times 50 \times 1.6\,\text{mm}^3$. All related parameters are labeled in Figure 2 and mentioned in Table 1.

3. THE PROPOSED ANTENNA DESIGN AND CONFIGURATION SEQUENCE

The schematic design procedure of the presented antenna is shown in Figure 3. As can be noticed, the antenna design is accomplished across three stages. The first stage includes the ring installation to form the antenna's radiator and impedance transformer construction to support the matching at 50 Ohms.

In the second stage, the modified Minkowski fractal curve is loaded to the ring to achieve the miniaturization and circular polarization for the proposed antenna synchronously. The sense of circular polarization is set by inserting a small gap in the ring to control the direction of the excitation current.

The third stage is concerned with the defected ground structure (DGS) etching to enhance the gain obtained from the antenna.

In terms of increasing the electrical current path, it is found that applying the modified Minkowski fractal curve on a circular ring patch could generate a new perimeter at each fractal's iteration, which is calculated by:

$$P_n = \left[1 + \left(2 \times F_{ec} \times \frac{L_f}{L_o}\right)\right] \times P_{n-1} + (F_{ec} \times W_f) \quad (1)$$

where F_{ec} is the number of effective fractal curves at each iteration, and L_o is the initial effective perimeter length before employment of the fractal, which will be equal to P_o. As for

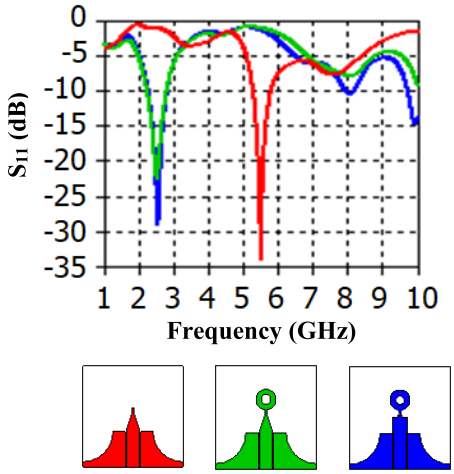

FIGURE 4. The effects of ring installation and impedance transformer construction on the proposed antenna's reflection coefficient behavior.

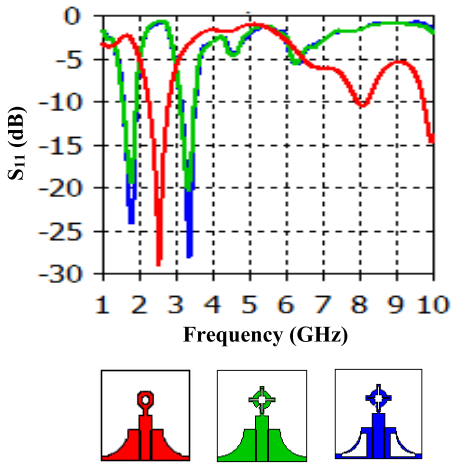

FIGURE 5. The effects of fractal loading and defected ground structure (DGS) etching on the proposed antenna's reflection coefficient behavior.

the circular ring of the presented antenna, L_o represents the half circumference of the circular ring or πR_{ou}.

Then, the lower resonant frequency achieved by the proposed antenna can be determined as:

$$F_{lr} = \frac{C_o}{L_{teff} \times \sqrt{\epsilon_{reff}}} \tag{2}$$

L_{teff} is defined as the total effective length or electrical current path that can be specified with the aid of the current distribution analysis to support fringing of the field on different regions along the structure of the designed antenna as a maximum flow of excitation current and thus could generate the lower resonant frequency. This length is formulated as:

$$L_{teff} = P_n + L_t + L_{fl} + 2L_g \tag{3}$$

4. PERFORMANCE EVALUATION OF THE PROPOSED ANTENNA

This section will present evaluations of the proposed antenna performance in terms of the various parameters characterizing its resulting responses.

4.1. Reflection Coefficient (S_{11}) & Axial Ratio (AR)

To study the details of antenna construction and clarify their effects on the obtainable reflection coefficient S_{11} from the designed antenna through different design stages till reaching the optimum structure as a proposed antenna in this communication, the reflection coefficients of the design stages are depicted in Figures 4 and 5.

Figure 4 shows the proposed antenna's reflection coefficient for three construction stages. The first stage's antenna without ring and impedance transformer could resonate with a band of frequencies around 5.5 GHz. The ring installation in the second stage minimizes the resonating band to around 2.5 GHz. The impedance transformer enhances the resonance at the lower band and supports the antenna to resonate with the other two bands, around 8 and 10 GHz.

The effects of fractal loading and defected ground structure etching are shown in Figure 5. The fractal increases the electrical current path along the circular ring. As a result, the designed antenna could resonate with two bands of frequencies, the lower band around 1.8 GHz and the upper band around 3.3 GHz. The use of the DGS technique reduces the reflection at the obtained resonating bands, which helps increase the proposed antenna's gain.

The simulated and measured reflection coefficients of the presented antenna are implied in Figure 6. For a swept frequency from 1 to 10 GHz, the proposed antenna achieves two resonating bands of frequencies. The first or lower band extends from 1.595 to 1.958 GHz, having a center frequency of 1.812 GHz and fractional bandwidth of 20.033%. The upper band covers frequencies from 3.164 to 3.55 GHz with a center frequency of 3.386 GHz and fractional bandwidth of 11.399%. Regarding the measured result, as can be seen, there is a good agreement with the result predicted by the simulation software, except that in the measured results, a poor impedance bandwidth below -10 dB appears as the third band around 8.3 GHz. This can be canceled due to the tolerances in manufacturing the designed antenna, which mainly represents very slight dimensions and takes place in some critical edge areas.

Figure 7 reveals the simulated and measured axial ratios of the designed antenna. As can be seen, a circular polarization property is verified for the lower operating band to cover frequency from 1.39–2.03 GHz with a 3-dB axial ratio bandwidth (ARBW) of 41.02%. As for the upper operating band, no axial ratio below 3-dB is satisfied; therefore, the radiation in this band is linearly polarized. To this result, the presented antenna has dual-polarized properties, and the sense of polarization can be obtained from far-field radiation pattern characteristics.

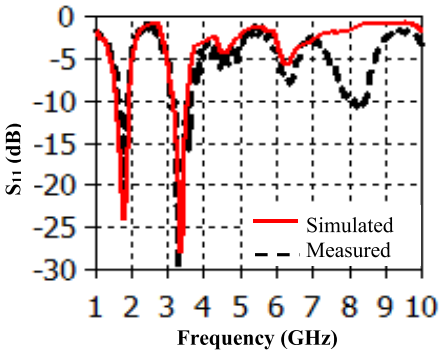

FIGURE 6. The simulated and measured input reflection coefficient of the designed antenna.

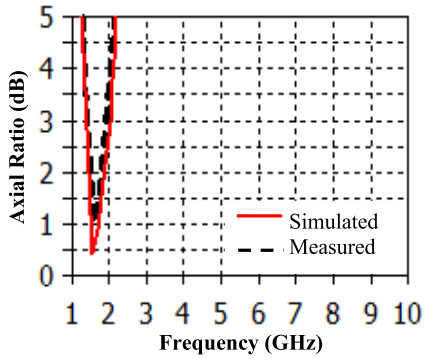

FIGURE 7. The simulated and measured Axial Ratio of the designed antenna.

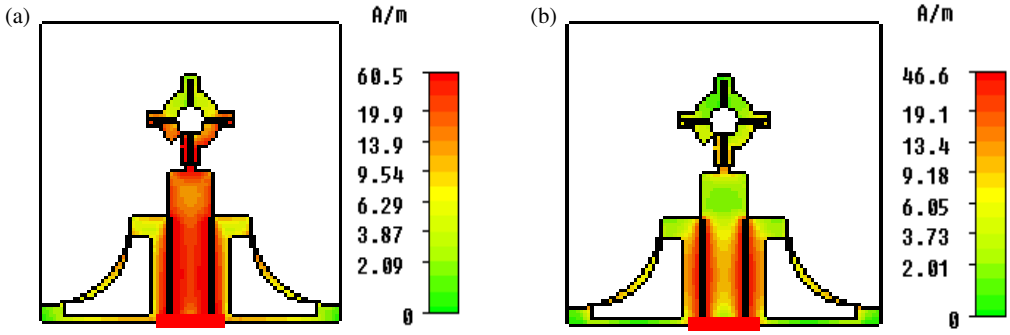

FIGURE 8. The simulated current distribution analysis of the designed antenna is at (a) 1.8 GHz and (b) 3.5 GHz.

4.2. Surface Current Distributions

The analysis of surface current distribution with the aid of the computer simulation technique (CST) tool is carried out and depicted in Figure 8 to illustrate the more effective lengths that cause minimum reflection in frequencies which are surrounded by the two obtained resonating bandwidths at the limit of ≤ -10 dB in the designed antenna.

Figure 8(a) shows the electrical current distribution on the surface of the proposed antenna at 1.8 GHz; it is clear that a large current flows along the feed line of the antenna and concentrates on three effective parts of fractal around the circular ring, so this concentration of the excitation current on these parts of fractal led to orthogonally flowing of it. Then, the circular polarization radiation characteristics are achieved for the lower resonating band.

The flow of the surface current at 3.5 GHz is shown in Figure 8(b). The effective regions that are responsible for generating this resonant frequency are the two gaps of the ungrounded co-planar waveguide (UCPW), so it has been found that the maximum amount of excitation current flows around these gaps.

The sense of circular polarization property can also be explored with the assistance of the 3D vector plot of the CST to animate current along the effective region at two different time instants by expressing the flow of the current with arrows and determining the resultant currents then comparing it to find out the direction of rotation as demonstrated in Figure 9. This figure displays the animated current through $t = 0°$ at the resonant frequency of 1.8 GHz. The intensity of the current is represented by arrow length along the surface of the effective regions for the designed antenna. When we compare the resultant $\overrightarrow{j_{sum}}$ with the other at $t = 90°$ in Figure 9(b) for the same frequency, we will find that the direction of rotation is clockwise. Therefore, the sense of polarization at this resonant frequency is left-handed circular polarization (LHCP).

4.3. Radiation Patterns

The designed antenna's simulated and measured 2D radiation patterns are plotted in phi $= 0°$ (XZ-plane) and phi $= 90°$ (YZ-plane) for two operating frequencies. Figure 10(a) presents the far-field radiation pattern at 1.8 GHz. In XZ-plane, the polarization is left-handed circular polarization in positive Z-direction and right-handed circular polarization (RHCP) in negative Z-direction, the cross-polarization level at $\theta = 0°$ between simulated and measured radiation patterns is about 20.6 dB. As for (YZ-plane), the polarization is left-handed circular polarization (LHCP) for any direction of θ, and the cross-level is 21 dB.

Figure 10(b) shows the radiation pattern of the designed antenna at 3.5 GHz to illustrate the co-polar and cross-polar radiations in both XZ and YZ planes for a linearly polarized resonating bandwidth. In the boresight direction, there is a difference about 18 dB between co-polarization and cross-polarization for the two dependent planes.

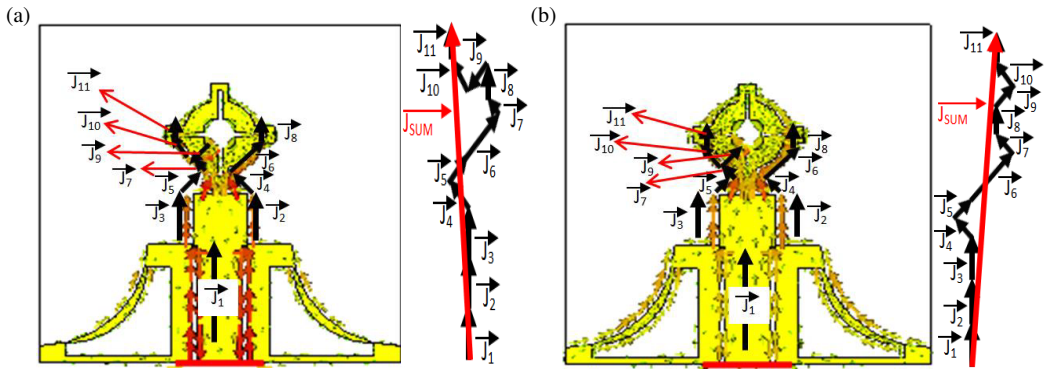

FIGURE 9. The animated current distribution on the surface of the designed antenna at 1.8 GHz through (a) $t = 0°$, and (b) $t = 90°$.

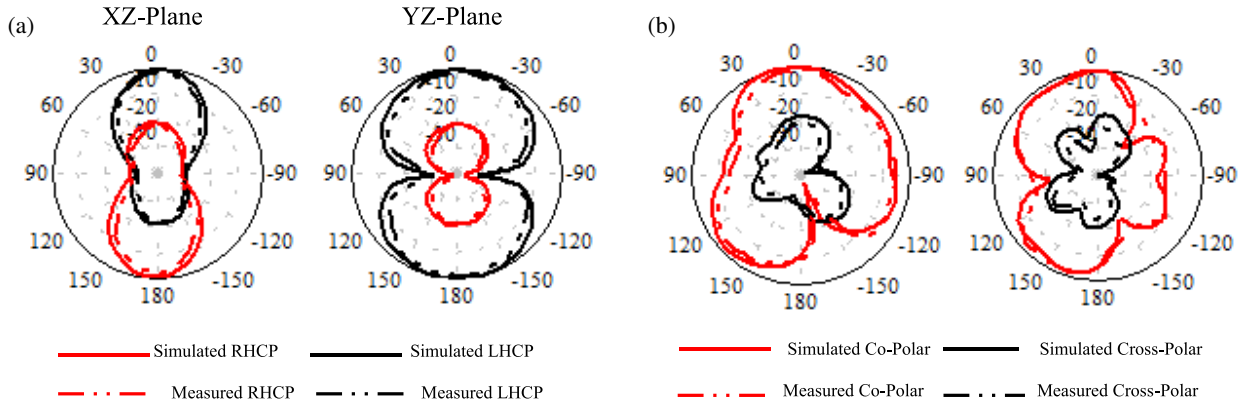

FIGURE 10. The simulated and measured 2D far-field radiation pattern of the designed antenna at (a) 1.8 GHz and (b) 3.5 GHz.

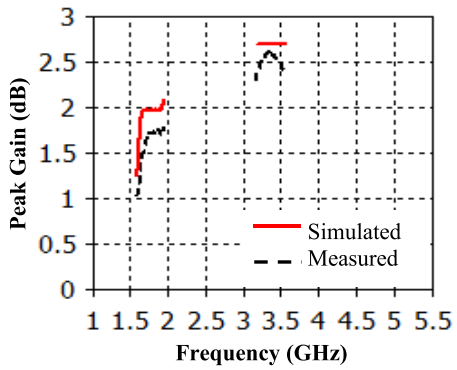

FIGURE 11. The designed antenna's simulated and measured peak gain is at (a) lower resonating and (b) upper resonating bandwidth.

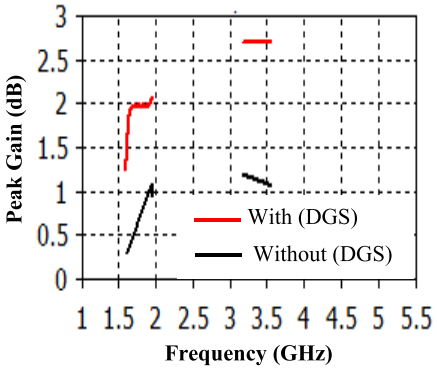

FIGURE 12. The effects of (DGS) on the peak gain obtained from the designed antenna at (a) lower band and (b) upper band.

4.4. The Gain

The peak gain for the two operating bandwidths of the proposed antenna is depicted in Figure 11 for both cases (simulated and measured results). The performed gain for the simulated lower resonating band is 1.25–2.09 dBi with a maximum peak gain of 2.09 dBi, and at the simulated upper resonating band it is 2.7 dBi throughout the band. The measured gain for the lower band is 1.04–1.79 dBi with a maximum peak gain of 1.79 dBi and for the upper band from 2.31–2.37 dBi with a maximum peak gain of 2.61 dBi.

Figure 12 demonstrates the effects of the defected ground structure (DGS) on the performed gain from the proposed antenna. As can be noticed, the DGS enhances the gain by 0.95 dBi at the lower band and increases the gain by more than 1.5 dBi at the upper band.

5. PARAMETRIC INVESTIGATION

The performance of the proposed antenna will be affected by the dimensions of many parameters that construct the optimum structure, as shown in Figure 2. These parameters provide a

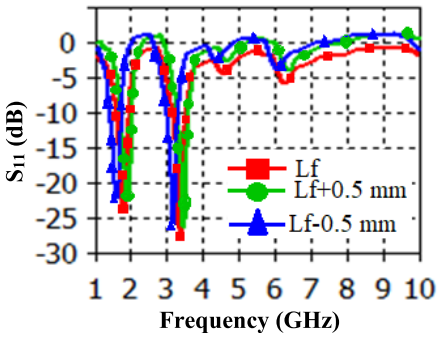

FIGURE 13. The effects of (L_f) on the reflection coefficient of the proposed antenna.

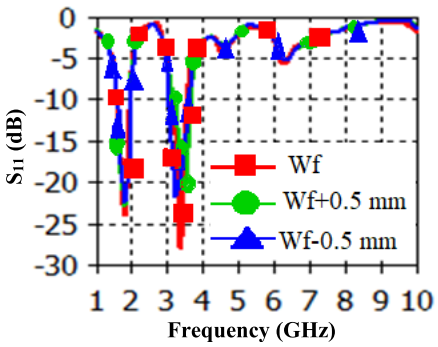

FIGURE 14. The effects of W_f on the reflection coefficient of the proposed antenna.

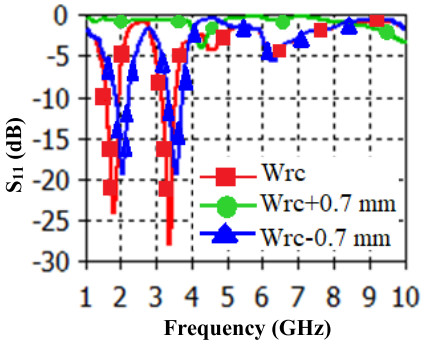

FIGURE 15. The effects of W_{rc} on the reflection coefficient of the proposed antenna.

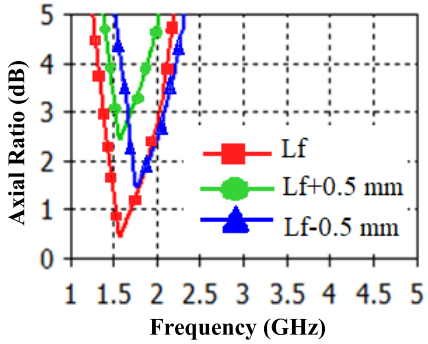

FIGURE 16. The effects of L_f on the axial ratio of the proposed antenna.

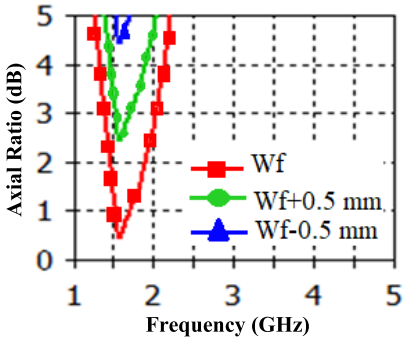

FIGURE 17. The effects of W_f on the axial ratio of the proposed antenna.

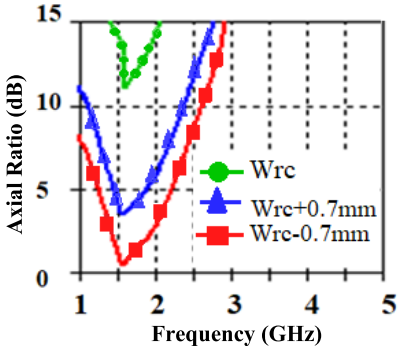

FIGURE 18. The effects of W_{rc} on the axial ratio of the proposed antenna.

free area, allowing the designer to perform the requirements. In this section, a study and analysis of more effective parameters to the response of the presented antenna are discussed with the aid of design software. Referring to the electrical current distribution and analysis in Figures 8 and 9, it is found that the fractal's external width and length, in addition to the gap slot, have a significant effect on the function of the impedance of the transformer and then the response of the designed antenna.

5.1. Reflection Coefficient S_{11}

5.1.1. The Effects of Fractal Length L_f

The effect of varying the modified Minkowski fractal L_f external length is demonstrated in Figure 13. The optimum dimension of L_f is 2.67 mm, and the variation of this value by 0.5 mm will cause an upper or lower shift to the center frequency of the two obtained resonating bandwidths.

5.1.2. The Effects of Fractal Width W_f

Figure 14 illustrates the response form of the designed antenna at different dimensions for the external fractal width W_r. So, the change of W_r by 0.5 mm increases the reflection at the upper resonating bandwidth and shifts its center frequency.

5.1.3. The Effects of Resonant Cavity Width W_{rc}

The resonant cavity slot is constructed by installing an impedance transformer between the ring (radiator of the antenna) and the feedline. The width of this slot represents the distance from the edge of the impedance transformer and the inner edge of the ground plane, which is about 0.05 mm. This slot has to control the excitation current that goes to the radiator of the designed antenna through its neck (impedance transformer). When the width of the resonant cavity is decreased close to zero, the antenna will not be able to radiate, and all available frequencies from 1–10 GHz will be reflected to the port. If the width is increased close to cancel the impedance transformer, it will weaken the matching and shift the two resonating bands to the upper frequencies, as in Figure 15.

5.2. Axial Ratio (AR)

5.2.1. The Effects of Fractal Length L_f

Adjusting the fractal structure L_f length satisfies the accepted axial ratio below 3-dB with suitable axial ratio bandwidth (ARBW) to cover the obtained resonating bandwidth. Still, if the value of L_f is increased by 0.5 mm, then the axial ratio will increase, and the ARBW will decrease. Also, the decrease of L_f will shift the obtained ARBW to the upper frequencies and reduce it, as shown in Figure 16.

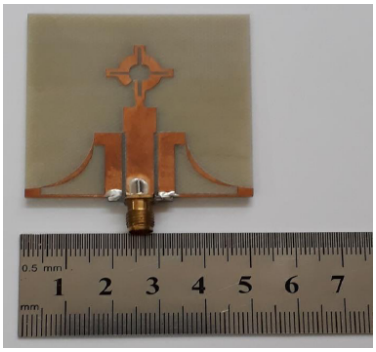

FIGURE 19. The fabricated antenna prototype.

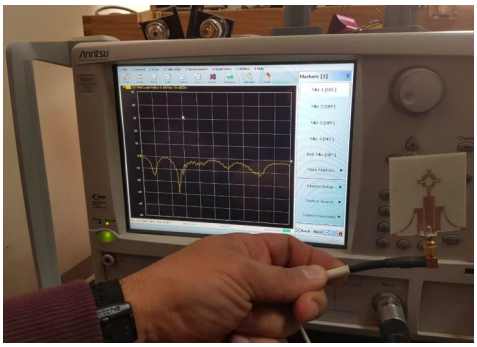

FIGURE 20. The measurement setup of the reflection coefficient for the fabricated antenna.

TABLE 2. Comparison table with other published works.

Ref	Fractal Type	Polarization	Resonating Band	Size of Antenna	Lower Resonant Frequency (GHz)
[1]	Minkowski and Koch curves (poly fractal)	Circular	Single	Substrate height $= 3.2$ mm	2.3
[2]	Minkowski and half-circled (poly fractal)	Circular	Triple	$50 \times 50 \times 3.2\,\text{mm}^3$	2.4
[3]	Minkowski and ring loaded (poly fractal)	Circular	Single	Radius $= 10$ mm, Substrate height $= 1.57$ mm	20
[4]	Minkowski fractal curve and Minkowski fractal structure (poly fractal)	Hybrid	Five Band	$51.9 \times 51.9 \times 1.6\,\text{mm}^3$	1.4
[5]	Giuseppe-Peano fractal (poly fractal)	Circular	Triple	$70 \times 70 \times 1.6\,\text{mm}^3$	1.47
[6]	Z-type fractal and Hilbert (poly fractal)	Circular	Triple	$57.24 \times 27 \times 1.6\,\text{mm}^3$	1.46
[7]	Koch and Minkowski pre-fractal (poly fractal)	Circular	Single	$70 \times 70 \times 1.5\,\text{mm}^3$	1.33
[8]	Minkowski fractal curve	Circular	Single	$42 \times 42 \times 4.5\,\text{mm}^3$	2.504
[9]	Minkowski fractal structure	Circular	Single	$55 \times 55 \times 1.6\,\text{mm}^3$	1.58
[10]	Flared-U-type asymmetrical fractal	Circular	Single	$50 \times 50 \times 3.2\,\text{mm}^3$	2.13
[11]	Gasper-Peano	Circular	Single	Substrate height $= 0.5$ mm	9
[12]	Fractal-rhombus slot	Circular	Single	$40 \times 40 \times 0.762\,\text{mm}^3$	3.74
[13]	Embedded slots fractal	Circular	Single	$80 \times 80 \times 1.6\,\text{mm}^3$	1.8
[14]	Spidron slot fractal	Circular	Single	$40 \times 40 \times 1.52\,\text{mm}^3$	2.47
[15]		Circular	Single	$45 \times 45 \times 3.18\,\text{mm}^3$	1.558
Prop. Ant.	Modified Minkowski fractal	Hybrid	Dual	$50 \times 50 \times 1.6\,\text{mm}^3$	1.595

5.2.2. The Effects of Fractal Width W_f

Figure 17 shows the effect of varying the fractal width W_f on the axial ratio of the proposed antenna. As seen, W_f is examined by increasing and decreasing its value by 0.5 mm. As a result of this examination, the generated axial ratio will diminish. The antenna will radiate a linearly polarized wave at the obtained resonating bandwidth instead of a circularly polarized wave before changing W_f.

5.2.3. The Effects of Resonant Cavity Width W_{rc}

The resonant cavity slot has a close relationship with the impedance transformer. Therefore, any variation in the slot's width will affect the impedance transformer's responsibility for

controlling the antenna's response by adjusting the amount of the excitation current and matching characteristics. So, from Figure 18, if W_{rc} is increased by 0.7 mm, it will distort the axial ratio because it will transgress the basic design for the ungrounded co-planar waveguide (UCPW) technique by canceling the two gaps around the feedline. Also, the decrease in the value of W_{rc} by 0.7 mm will cancel the impedance transformer from the designed antenna structure, and this leads to the weakening of the axial ratio because the antenna and in this case, will lose the matching property.

The designed antenna structure depicted in Figure 2 is fabricated on an FR4 substrate with a relative permittivity of 4.4 and thickness of 1.6 mm. The photo of the fabricated prototype is shown in Figure 19. The input reflection coefficient is measured using a broadband vector network analyzer (VNA) type VectorStar (ME7838A), as shown in Figure 20. Ultimately, for the purpose of highlighting the most important advantages in this antenna, a comparison was made with a number of published works that dealt with the same topic, as in Table 2.

6. CONCLUSION

A compact dual-band dual-polarized antenna is investigated and analyzed thoroughly in this paper. The reduction in size for the proposed antenna is made by adopting a new approach, which is the employment of the modified Minkowski fractal of 1st iteration on an open ring to form the radiator of the antenna that is fed by an ungrounded co-planar waveguide (UCPW) and supported by impedance transformer besides with the defected ground structure (DGS) technique. The proposed antenna achieves a lower band from 1.595 to 1.958 GHz with circular polarization property suitable for GSM application. The upper band has linear polarization covering frequencies from 3.164 to 3.55 which is suitable for WiMax application. The proposed antenna results are evaluated using a computer simulation technique (CST) microwave studio. A parametric study is conducted to show the effects of more crucial parameters on the response of the designed antenna. The measurements obtained from the fabricated antenna agree well with the predicted simulated results.

REFERENCES

[1] Reddy, V. V. and N. V. S. N. Sarma, "Single feed circularly polarized poly fractal antenna for wireless applications," *International Journal of Computer and Information Engineering*, Vol. 8, No. 11, 1710–1713, 2014.

[2] Reddy, V. V. and N. V. S. N. Sarma, "Single layer single probe feed circularly polarized triple band fractal boundary microstrip antenna for wireless applications," *International Journal of Microwave and Wireless Technologies*, Vol. 9, No. 3, 657–664, 2017.

[3] Raj, S., N. Kishore, G. Upadhyay, S. Tripathi, and V. S. Tripathi, "A compact design of circularly polarized fractal patch antenna for 5G application," in *IEEE MTT-S International Microwave and RF Conference (IMaRC)*, 1–4, 2018.

[4] Das, S. and S. Sahu, "Square fractal ring loaded CPW-fed circular polarized antenna," in *IEEE Region 10 Conference (TENCON)*, 1556–1559, Singapore, Nov. 2016.

[5] Oraizi, H. and S. Hedayati, "Circularly polarized multiband microstrip antenna using the square and Giuseppe Peano fractals," *IEEE Transactions on Antennas and Propagation*, Vol. 60, No. 7, 3466–3470, Jul. 2012.

[6] Oraizi, H. and S. Hedayati, "Application of Z-type and Hilbert fractal structures for multiband and circularly polarized microstrip antennas," in *IEEE 15th Mediterranean Microwave Symposium (MMS)*, Lecce, Italy, Nov. 2015.

[7] Hua, X. and D. Yang, "Circularly polarized antenna with a fractal boundary and Y-type strip," in *IEEE 2nd Information Technology, Networking, Electronic and Automation Control Conference (ITNEC)*, 788–791, Dec. 2017.

[8] Kotla, S., V. Shivani, M. Ashish, and S. Kumar, "Compact circularly polarized fractal patch antenna using defected ground structure," in *TEQIP III Sponsored International Conference on Microwave Integrated Circuits, Photonics and Wireless Networks (IMICPW)*, 29–33, 2019.

[9] Joy, S., S. Natarajamani, and S. M. Vaitheeswaran, "Minkowski fractal circularly polarized planar antenna for GPS application," in *8th International Conference on Advances in Computing and Communication (ICACC)*, Vol. 143, 66–73, Kochi, India, Sep. 2018.

[10] Reddy, V. V., "Single-feed circularly polarized flared-U fractal boundary microstrip antenna," *IETE Journal of Research*, Vol. 63, No. 4, 577–587, 2017.

[11] Rajabloo, H. and J. Mandali Jr., "Microstrip Gasper-Peano fractal antenna for circular polarization applications," *Microwave and Optical Technology Letters*, Vol. 61, No. 6, 1622–1627, Jun. 2019.

[12] Zhong, S.-S. and L.-N. Zhang, "Miniaturized circularly-polarized fractal-rhombus slot antenna," in *IEEE International Symposium on Antennas and Propagation (APSURSI)*, 802–805, Spokane, WA, Jul. 2011.

[13] Chaouki, G., A. Ferchichi, and A. Gharsallah, "A fractal circular polarized RFID tag antenna," *Central European Journal of Engineering*, Vol. 3, 446–450, 2013.

[14] Altaf, A., Y. Yang, K.-Y. Lee, and K. C. Hwang, "Wideband circularly polarized spidron fractal slot antenna with an embedded patch," *International Journal of Antennas and Propagation*, Vol. 2017, 2017.

[15] Wei, K., J. Y. Li, L. Wang, R. Xu, and Z. J. Xing, "A new technique to design circularly polarized microstrip antenna by fractal defected ground structure," *IEEE Transactions on Antennas and Propagation*, Vol. 65, No. 7, 3721–3725, Jul. 2017.

[16] Hatem, G. M., A. J. Salim, T. A. Elwi, H. T. Ziboon, and J. K. Ali, "Wunderlich curve fractal dipole antenna for dual-band wearable RFID applications," *Journal of Engineering and Applied Sciences*, Vol. 14, No. 4, 1093–1099, 2019.

[17] Yassen, M. T., M. R. Hussan, H. A. Hammas, A. J. Salim, and J. K. Ali, "Design of compact dual-band fractal monopole antenna with virtually extended ground plane," *Advanced Electromagnetics*, Vol. 7, No. 4, 19–26, 2018.

[18] Ali, J. K., A. J. Salim, A. I. Hammoodi, and H. Alsaedi, "An ultra-wideband printed monopole antenna with a fractal based reduced ground plane," in *Progress In Electromagnetics Research Symposium Proceedings*, 613–617, Moscow, Russia, Aug. 2012.

[19] Kazemi, F., "Dual band compact fractal THz antenna based on CRLH-TL and graphene loads," *Optik*, Vol. 206, 164369, Mar. 2020.

[20] Hua, X., D. Yang, and D. Geng, "A new type of dual-band circularly polarized antenna based on fractal structure," in *2017 IEEE Asia Pacific Microwave Conference (APMC)*, 787–790, Kuala Lumpur, Malaysia, Nov. 2017.